Crystallizing Kagome Artificial Spin Ice

Wen-Cheng Yue, Zixiong Yuan, Yang-Yang Lyu, Sining Dong, Jian Zhou, Zhi-Li Xiao, Liang He, Xuecou Tu, Ying Dong, Huabing Wang, Weiwei Xu, Lin Kang, Peiheng Wu, Cristiano Nisoli, Wai-Kwong Kwok, and Yong-Lei Wang

Phys. Rev. Lett. **129**, 057202 — Published 29 July 2022

DOI: 10.1103/PhysRevLett.129.057202

Crystallizing Kagome artificial spin ice

Wen-Cheng Yue[1,2,+], Zixiong Yuan[1,2,+], Yang-Yang Lyu[1], Sining Dong[1,*], Jian Zhou[2], Zhi-Li Xiao[3,4,*], Liang He[2], Xuecou Tu[1,5], Ying Dong[6], Huabing Wang[1,5,*], Weiwei Xu[1], Lin Kang[1,5], Peiheng Wu[1,5], Cristiano Nisoli[7], Wai-Kwong Kwok[3], and Yong-Lei Wang[1,2,5,*]

[1]Research Institute of Superconductor Electronics, School of Electronic Science and Engineering, Nanjing University, Nanjing, 210023, China

[2]Jiangsu Provincial Key Laboratory of Advanced Photonic and Electronic Materials, School of Electronic Science and Engineering, Nanjing University, Nanjing 210093, China

[3]Materials Science Division, Argonne National Laboratory, Argonne, Illinois 60439, USA

[4]Department of Physics, Northern Illinois University, DeKalb, Illinois 60115, USA

[5]Purple Mountain Laboratories, Nanjing, 211111, China

[6]Research Center for Quantum Sensing, Zhejiang Lab, Hangzhou, Zhejiang, 311121, China

[7]Theoretical Division and Center for Nonlinear Studies, Los Alamos National Laboratory, Los Alamos, New Mexico 87545, USA

Artificial spin ices are engineered arrays of dipolarly coupled nanobar magnets. They enable direct investigations of fascinating collective phenomena from their diverse microstates. However, experimental access to ground states in the geometrically frustrated systems has proven difficult, limiting studies and applications of novel properties and functionalities from the low energy states. Here, we introduce a convenient approach to control the competing diploar interactions between the neighboring nanomagnets, allowing us to tailor the vertex degeneracy of the ground states. We achieve this by tuning the length of selected nanobar magnets in the spin ice lattice. We demonstrate the effectiveness of our method by realizing multiple low energy microstates in a Kagome artificial spin ice, particularly the hardly accessible long range ordered ground state – the spin crystal state. Our strategy can be directly applied to other artificial spin systems to achieve exotic phases and explore new emergent collective behaviors.

Artificial spin ices (ASIs) are exemplar material-by-design systems with intriguing physical phenomena such as geometrical frustration [1–6], monopole-like excitations [7–10], Coulomb phase [10,11] and phase transitions [12–14]. They lead to novel functionalities with great potential for applications, such as low-power data storage [15], encryption devices [16] and advanced computations [17–19]. As one of the simplest ASI structures, the Kagome ASI has attracted extensive attention [2,7–9,12,13,20–29], because it is highly frustrated and contains a rich phase diagram. Theoretical investigations suggest four thermal phases with reducing temperatures [13,21,28,30]: a high temperature paramagnetic state (PM phase); a spin liquid with correlated spins satisfying the Kagome ice rule (‘two in/one out’ or ‘two out/one in’) but with neither charge nor spin ordering (SL1 phase); a long-range ordered charge crystal in a disordered spin liquid state (SL2 phase); as well as a spin crystal state in which the spins have long-range ordering (LRO phase) as the lowest temperature state. These thermal phases were used to understand the temperature dependent magnetotransport results in honeycomb structures of nanowire networks (which is sometimes also called Kagome ASI, because the moments of the nanowires satisfy the Kagome ice rule), where the LRO spin crystal state may contribute to the topological Hall signals at the lowest temperatures [30]. However, previous investigations have shown that direct experimental access of the spin crystal states of a Kagome ASI is challenging [12,31]. With the exception of the magnetic writing approach [31], no LRO spin crystal state has been unambiguously visualized in a Kagome ASI consisting of fully disconnected nanobar magnets, hindering investigations of emergent phenomena and phase transitions from its low energy manifolds.

The collective properties of ASIs are directly associated with their lattice geometries, and are intimately governed by the competing dipolar interactions between their constituent elements, i.e., the single-domain nanobar magnets [16,32–34]. The difficulty of obtaining the LRO state of a Kagome ASI originates from the extensive degeneracy of the ground state, resulting from the high frustration of the tri-leg vertices. The ground state of a Kagome ASI exhibits neither charge nor spin order when only nearest-neighbor interactions are considered [21,35]. Further-neighbor interactions induce charge and/or spin ordering [13,21,28]. However, these longer-distance interactions are much weaker than that from the nearest-neighbor. As a result, the properties of artificial spin ices are mostly dominated by the nearest-neighbor interactions. Recently, utilizing the micromagnetic nature of connected vertices in the honeycomb structure of nanowire networks, the LRO spin crystal phase of Kagome ices was realized for the first time, in which notches were introduced to reduce the vertex degeneracy [36]. More recently, asymmetric bridges were introduced to break the six-fold symmetry of Kagome ASI's vertices, leading to a direct real-space imaging of the phase transitions [37]. However, these strategies are not applicable to Kagome ASIs consisting of disconnected nanobar magnets. In this letter, we develop a new method to tailor the vertex degeneracy and the ground states of a Kagome ASI of disconnected magnetic nanobars, and we directly present the phase transition from the SL1 liquid to LRO crystal state. Unlike the recently realized connected Kagome ASI structure [36,37], in which the coupling is dominated by short range exchange interaction, our disconnected ASIs maintain their long range dipolar interaction, therefore, allowing us to directly evaluate the critical role of the nearest and/or next nearest neighbor interactions, which is crucial for understanding the phase transitions between the various low energy manifolds of ASIs.

In square ASIs, the six vertex configurations satisfying the spin ice-rule are divided into two types according to energy [1,2,10,11,14,17,18,22,24,29,38–44]. The lowest energy configuration is two-fold degenerate, leading to the formation of a long-range ordered ground state [1,38–41]. The low degeneracy of 2 in a square ASI is induced by the non-equal interactions between the nanobar magnets at each vertex. Following this notion, we developed a method to achieve the LRO spin ice state of a regular Kagome ice by inducing non-equal interactions between the three nanobar magnets at a vertex, which reduces the ground state degeneracy of a Kagome vertex from 6 to 2. As shown in Fig. 1(a), we increase the length of one of the three nanobar magnets (α) in each vertex, while maintaining the length of the other two magnets (β) and the lattice constant (see Fig. S1 of Supplemental Material for the detailed arrangement of α and β magnets in the lattice [45]). This breaks the three-fold rotation symmetry of the vertex. The interactions between the three nanobar magnets at each vertex are no longer equivalent. As shown in Fig. 1(b), the original six-fold degenerate vertices are divided into two groups of Type K-I and K-II configurations with different energies. We denote the interaction energy of the frustrated magnet pair between two β nanomagnets in Type K-I vertices as J_1, while that between α and β nanomagnets in Type K-II vertices as J_2 [Fig. 1(b)]. Since each vertex satisfying the Kagome ice rule contains only one frustrated magnet pair, J_1 and J_2 also represent the energies of the Type K-I and K-II vertices, respectively. Because the endpoints of the lengthened α nanomagnet are closer to the vertex center, J_1 is lower than J_2, resulting in the two-fold degenerate Type K-I vertices to be the ground state configuration. As shown in Fig. 1(a), when all the vertices are satisfied to be in the Type K-I ground state configuration, a LRO spin crystal emerges. We can further tailor the energy difference between Type K-I and K-II vertices by varying the length (L_α) of the α

nanomagnet. Figure 1(c) presents the vertex energy evolution of Type K-I and K-II vertices as a function of L_α, calculated from micromagnetic simulation using Mumax3 [46]. It shows that J_2 increases with L_α while J_1 remains constant. Thus, the energy difference J_2- J_1 between Type K-I and K-II vertices increases with L_α. Therefore, varying the length of the α nanomagnets allows us to regulate the effective temperature, similar to the effect of tuning the vertex notch in the connected honeycomb structures [36]. This enables us to tailor the phases in a fully disconnected Kagome ASI.

To experimentally validate this approach, we fabricated Kagome ASIs with Permalloy nanomagnets and with a series of L_α values (220 nm, 270 nm, 320 nm, 370 nm, 420 nm and 440 nm) for the α nanomagnets (see SEM images in Fig. S2 of Supplemental Material [45]). The length (L_β) of the β magnets is fixed at 220 nm, and the lattice constant is a = 640 nm for all samples [Fig. 1(a)]. The width and thickness of all the nanomagnets are 80 nm and 15 nm, respectively. Details of the sample fabrication process and parameters can be found in Supplemental Material [45]. A demagnetization procedure (see Supplemental Material [45]) lasting 72 hours was performed to obtain the low-energy states [11,47]. Figures 1(d) and 1(e) show the SEM images of the samples with L_α = 220 nm and 420 nm, respectively. The corresponding magnetic force microscopy (MFM) images are displayed in Figs. 1(f) and 1(g), respectively, which allow us to determine the magnetic moment (or spin) configurations [see arrows in Figs. 1(f) and 1(g)]. The results show that all the vertices in all measured samples satisfy the Kagome ice rule ('two in/one out' or 'two out/one in'). This indicates our demagnetization procedure successfully brought the samples into the low energy ice rule manifold. The conventional Kagome ASI with $L_\alpha = L_\beta$ [Fig. 1(d)] exhibits disordered spin and charge configurations [Fig. 1(f)], consistent with the frozen spin liquid SL1 state. In contrast, the modified Kagome ASI with $L_\alpha > L_\beta$ (Fig. 1e) exhibits perfect spin and charge ordering [Fig.

1(g)], leading to a successful realization of the LRO spin crystal ground state.

The transition from SL1 phase to LRO spin crystal phase is demonstrated by the MFM images of samples with increasing L_α values in Figs 2(a-f). The corresponding maps of vertex distributions in Figs. 2(g-l) shows that domains of crystallization become larger with L_α. For the sample with L_α = 220 nm (the conventional Kagome ASI), the Type K-I and K-II vertices are degenerate, leading to a disordered magnetic state with vertex populations of 33.75% and 66.25% for Type K-I and K-II vertices, respectively. This is consistent with the configurational (or random) populations of 1/3 and 2/3 for Type K-I and K-II vertices, as expected for a spin liquid, and proves that our demagnetization procedure effectively brought the system into an effective thermal equilibrium state. When $L_\alpha > 220$ nm, the Type K-II vertices become an excited state. With increasing L_α, the energy difference between Type K-I and Type K-II vertices increases [Fig. 1(c)] and thus the population of Type K-I vertices gradually increases. As shown in Figs. 2(g-l), ordered domains of Type K-I vertices emerge and grow with increasing L_α. For the sample with large L_α, such as 440 nm [Fig. 2(l)], 93% of the vertices are in the Type K-I ground state, and domain walls comprised of excited Type K-II vertices (red) are clearly visible. These results match nicely with our Monte Carlo simulations (Figs. S3 and S4 of Supplemental Material [45]) conducted using a thermal annealing protocol and considering only nearest-neighbor interactions (see Supplemental Material [45]). This suggests that the transition from SL1 phase to LRO spin crystal state is dominated by the nearest-neighbor interactions.

We can further elucidate the phase transition from liquid to crystal using magnetic structure factors [11, 47]. Maps of the magnetic spin structure factor are shown in Figs. 2(m-r). For the conventional Kagome ASI ($L_\alpha = 220$ nm), the magnetic spin structure factor map shows structured diffusive pattern [Fig. 2(m)], consistent with previous results of SL1 phase [13,36]. With gradually increasing L_α, we can clearly observe the emergence and enhancement of Bragg peaks [Figs. 2(o-r)]. These Bragg peaks show split-peak structures whose number reduces with increasing L_α, as shown in the insets of Figs. 2(o-r). These split Bragg peaks originate from scattering between domains, as demonstrated by the structure factor maps of the artificial domain configurations in Fig. S5 of Supplemental Material [45]. The number of domains decreases when they merge, resulting in reduced number of split Bragg peaks. This suggests that the texture of Bragg peaks could be used as a qualitative parameter to investigate ordering and domain formation in ASIs, e.g., we could estimate the relative sizes of domains from the number of split Bragg peaks.

Previous investigations of conventional Kagome ASIs revealed local ordering of magnetic charges [22–24]. Figs. 3(a-f) are maps of magnetic charge configurations corresponding to the spin and/or vertex configurations in Figs. 2(g-l). We can see that the charge domains of the two-fold degenerate phases (green and yellow) grow with increasing L_α. When comparing the charge distributions to the vertex or spin distributions, we can see that their profiles match very well with each other for the samples with large L_α values [Figs. 2(i-l) and 3(c-f)], i.e., the charge ordering is embedded in the spin ordering for spin crystal state. However, the charge and vertex distributions deviate as the number of Type K-II vertices increases [Figs. 2(g) and 3(a)]. A similar behavior is observed when we compare the magnetic spin structure factor maps with the magnetic charge structure factor maps. For large L_α, both spin [Fig. 2(o-r)] and charge [Fig. 3(i-l)] structure factor maps exhibit clear Bragg peaks with the same peak splitting [insets of Fig. 2(o-r) and Fig. 3(i-l)]. However, for small L_α values, e.g., for the conventional Kagome ASI with $L_\alpha = L_\beta = 220$ nm, the spin structure factor map is structured but diffusive [Fig. 2(m) and 2(n))], while in contrast, the charge structure factor maps display clear Bragg peaks, although they are broad [Fig. 3(g) and 3(h)]. This indicates the emergence of charge ordering in the spin liquid state. As mentioned earlier, charge ordering should not appear when there are only nearest-neighbor interactions and the six-fold symmetry is not broken [21,35]. Our Monte Carlo simulations with only nearest-neighbor interactions show that there are no Bragg peaks in the magnetic charge structure factor map for conventional Kagome ASI (Fig. S6g of Supplemental Material [45]). This suggests that further-neighbor interactions beyond nearest-neighbors play a role in the liquid state. On the other hand, the consistency between experiment [Fig. 3(i-l)] and simulation (Fig. S6(i-l) of Supplemental Material [45]) for samples with large L_α unambiguously suggests the LRO spin crystal phase can be established with only nearest-neighbor interactions.

We have shown that the local interactions of an ASI have significant impact on their collective behavior and ultimately affect the properties of the entire system. The length of selective nanobar magnets can be used as a convenient knob to tune the local coupling strength, which enables us to access various low-energy manifolds and phase transitions in a fully disconnected ASI. We proved that although the next-nearest neighbor interaction plays a notable role through the magnetic charge structure factor maps, the crystallization of the Kagome ice structure with reduced vertex degeneracies is dominated only by the nearest neighbor interaction. This method could be used to manipulate the frustration in ASIs for attaining even more exotic ground state phases (see Figs. S7 of Supplemental Material [45]). It would also allow us to realize new magnetic configurations that are hard to access with magnetization method, e.g., to design novel ASIs with composite ground states in which different low energy states co-exist in the same sample, as illustrated by the hybrid ground state of both liquid and crystal in Fig. S8 of Supplemental Material [45]. This would allow us to investigate phase transitions between these new types of low energy states. Furthermore, kinetics becomes topologically protected in the SL2 phase and in the LRO state [48], and our structural modifications can be employed to fine-tune different kinetic regimes in thermal realizations or under field inversions. In addition, this method is also applicable to other types of artificial spin ices, leading to new opportunities to explore more exotic collective phenomena, such as novel phases and phase transitions. It could also be combined with the other structure modification strategies, such as lattice transformation [49,50], to design new ASIs with controllable degeneracies. This method, maintaining the dipolar coupling between disconnected nanomagnets, could result in different spin dynamic properties and magnonic applications [51,52] than those in connected systems [36,37]. Moreover, our approach avoids complex analysis of the micromagnetic structures such as the domains/domain-walls in the vertices of connected systems, and thus offers a simpler Kagome model which can connect with a variety of systems outside of magnetism, such as metal organic frameworks [53] and mechanical metamaterials [54, 55]. Last but not least, the observed Bragg peaks' splitting induced by spin scattering between domains could lead to an alternative way to investigate domain/domain wall formation in ASIs.

Figure captions

Fig.1. Tunable Kagome artificial spin ice. (a) Design of tunable Kagome artificial spin ice with extended length L_α of α magnets and fixed length L_β of β nanomagnets. (b) Six low energy vertex configurations satisfying the Kagome ice rule are separated into two groups based on energies. J_1 and J_2 are the coupling strengths of frustrated magnet pairs. (c) Evolution of the vertex energies as a function of L_α. (d) and (e) SEM images of Kagome artificial spin ices with L_α = 220 nm (d) and L_α = 420 nm (e), respectively. Scale bar, 500 nm. (f) and (g) MFM images corresponding to (d) and (e), respectively. Arrows indicate spin configurations. Scale bar, 500 nm.

Fig.2. Transition from liquid to crystal. (a)-(f) MFM images for samples with various L_α values, respectively. Scale bar, 2 μm. (g)-(l) spin configurations and vertex distributions extracted from (a)-(f). Type K-I and K-II vertices are shown in blue and red, respectively. (m)-(r) corresponding maps of magnetic structure factors calculated respectively from the spin configurations in (g)-(l). Insets of (o)-(r) show expanded views of the split Bragg peaks.

Fig.3. Magnetic charge ordering. (a)-(f) magnetic charge distributions corresponding to MFM images in Figs. 2(a)-2(f) respectively. Green and yellow denote two phases of magnetic charge ordering. Scale bar, 2 μm. (g)-(l) maps of magnetic charge structure factors associated with (a)-(f). Insets show expanded views of the split Bragg peaks.

Acknowledgment

This work is supported by the National Key R&D Program of China (2018YFA0209002 and 2021YFA0718802), the National Natural Science Foundation of China (61771235, 61971464, 61727805, 11961141002, 62101243), Jiangsu Excellent Young Scholar program (BK20200008) and Jiangsu Shuangchuang program. Part of the project design (Z.L.X.) and manuscript writing (Z.L.X. and W.K.K.) are supported by the U.S. Department of Energy, Office of Science, Basic Energy Sciences, Materials Sciences and Engineering. Z.L.X. also acknowledges support from the National Science Foundation under Grant No. DMR-1901843 for his efforts on data analysis. Y.D. acknowledges support from the Major Scientific Research Project of Zhejiang Lab (2019MB0AD01), the Center initiated Research Project of Zhejiang Lab (2021MB0AL01) and the Major Project of Natural Science Foundation of Zhejiang Province (LD22F050002).

+ Authors contribute equally

* Correspondence to: sndong@nju.edu.cn; xiao@anl.gov; hbwang@nju.edu.cn; yongleiwang@nju.edu.cn

References

[1] R. F. Wang, C. Nisoli, R. S. Freitas, J. Li, W. McConville, B. J. Cooley, M. S. Lund, N. Samarth, C. Leighton, V. H. Crespi, and P. Schiffer, *Artificial "spin Ice" in a Geometrically Frustrated Lattice of Nanoscale Ferromagnetic Islands*, Nature **439**, 303 (2006).

[2] C. Nisoli, J. Li, X. Ke, D. Garand, P. Schiffer, and V. H. Crespi, *Effective Temperature in an Interacting Vertex System: Theory and Experiment on Artificial Spin Ice*, Phys. Rev. Lett. **105**, 047205 (2010).

[3] M. J. Morrison, T. R. Nelson, and C. Nisoli, *Unhappy Vertices in Artificial Spin Ice: New Degeneracies from Vertex Frustration*, New J. Phys. **15**, 045009 (2013).

[4] G. W. Chern, M. J. Morrison, and C. Nisoli, *Degeneracy and Criticality from Emergent Frustration in Artificial Spin Ice*, Phys. Rev. Lett. **111**, 177201 (2013).

[5] I. Gilbert, G. W. Chern, S. Zhang, L. O'Brien, B. Fore, C. Nisoli, and P. Schiffer, *Emergent Ice Rule and Magnetic Charge Screening from Vertex Frustration in Artificial Spin Ice*, Nat. Phys. **10**, 670 (2014).

[6] I. Gilbert, Y. Lao, I. Carrasquillo, L. O'brien, J. D. Watts, M. Manno, C. Leighton, A. Scholl, C. Nisoli, and P. Schiffer, *Emergent Reduced Dimensionality by Vertex Frustration in Artificial Spin Ice*, Nat. Phys. **12**, 162 (2016).

[7] S. Ladak, D. E. Read, G. K. Perkins, L. F. Cohen, and W. R. Branford, *Direct Observation of Magnetic Monopole Defects in an Artificial Spin-Ice System*, Nat. Phys. **6**, 359 (2010).

[8] E. Mengotti, L. J. Heyderman, A. F. Rodríguez, F. Nolting, R. V. Hügli, and H. B. Braun,

Real-Space Observation of Emergent Magnetic Monopoles and Associated Dirac Strings in Artificial Kagome Spin Ice, Nat. Phys. **7**, 68 (2011).

[9] R. V. Hügli, G. Duff, B. O'Conchuir, E. Mengotti, A. Fraile Rodríguez, F. Nolting, L. J. Heyderman, and H. B. Braun, *Artificial Kagome Spin Ice: Dimensional Reduction, Avalanche Control and Emergent Magnetic Monopoles*, Phil. Trans. R. Soc. A. **370**, 5767 (2012).

[10] A. Farhan, M. Saccone, C. F. Petersen, S. Dhuey, R. V. Chopdekar, Y. L. Huang, N. Kent, Z. Chen, M. J. Alava, T. Lippert, A. Scholl, and S. van Dijken, *Emergent Magnetic Monopole Dynamics in Macroscopically Degenerate Artificial Spin Ice*, Sci. Adv. **5**, eaav6380 (2019).

[11] Y. Perrin, B. Canals, and N. Rougemaille, *Extensive Degeneracy, Coulomb Phase and Magnetic Monopoles in Artificial Square Ice*, Nature **540**, 410 (2016).

[12] L. Anghinolfi, H. Luetkens, J. Perron, M. G. Flokstra, O. Sendetskyi, A. Suter, T. Prokscha, P. M. Derlet, S. L. Lee, and L. J. Heyderman, *Thermodynamic Phase Transitions in a Frustrated Magnetic Metamaterial*, Nat. Commun. **6**, 8278 (2015).

[13] B. Canals, I. A. Chioar, V. D. Nguyen, M. Hehn, D. Lacour, F. Montaigne, A. Locatelli, T. O. Menteş, B. S. Burgos, and N. Rougemaille, *Fragmentation of Magnetism in Artificial Kagome Dipolar Spin Ice*, Nat. Commun. **7**, 11446 (2016).

[14] O. Sendetskyi, V. Scagnoli, N. Leo, L. Anghinolfi, A. Alberca, J. Lüning, U. Staub, P. M. Derlet, and L. J. Heyderman, *Continuous Magnetic Phase Transition in Artificial Square Ice*, Phys. Rev. B **99**, 214430 (2019).

[15] M. T. Kaffash, S. Lendinez, and M. B. Jungfleisch, *Nanomagnonics with Artificial Spin Ice*, Phys. Lett. A **402**, 127364 (2021).

[16] S. H. Skjærvø, C. H. Marrows, R. L. Stamps, and L. J. Heyderman, *Advances in Artificial Spin Ice*, Nat. Rev. Phys. **2**, 13 (2020).

[17] H. Arava, P. M. Derlet, J. Vijayakumar, J. Cui, N. S. Bingham, A. Kleibert, and L. J. Heyderman, *Computational Logic with Square Rings of Nanomagnets*, Nanotechnology **29**, 265205 (2018).

[18] H. Arava, N. Leo, D. Schildknecht, J. Cui, J. Vijayakumar, P. M. Derlet, A. Kleibert, and L. J. Heyderman, *Engineering Relaxation Pathways in Building Blocks of Artificial Spin Ice for Computation*, Phys. Rev. Appl. **11**, 054086 (2019).

[19] F. Caravelli and C. Nisoli, *Logical Gates Embedding in Artificial Spin Ice*, New J. Phys. **22**, 103052 (2020).

[20] N. Rougemaille, F. Montaigne, B. Canals, A. Duluard, D. Lacour, M. Hehn, R. Belkhou, O. Fruchart, S. El Moussaoui, A. Bendounan, and F. MacCherozzi, *Artificial Kagome Arrays of Nanomagnets: A Frozen Dipolar Spin Ice*, Phys. Rev. Lett. **106**, 057209 (2011).

[21] G. W. Chern, P. Mellado, and O. Tchernyshyov, *Two-Stage Ordering of Spins in Dipolar Spin Ice on the Kagome Lattice*, Phys. Rev. Lett. **106**, 207202 (2011).

[22] S. Zhang, I. Gilbert, C. Nisoli, G. W. Chern, M. J. Erickson, L. O’Brien, C. Leighton, P. E. Lammert, V. H. Crespi, and P. Schiffer, *Crystallites of Magnetic Charges in Artificial Spin Ice*, Nature **500**, 553 (2013).

[23] I. A. Chioar, B. Canals, D. Lacour, M. Hehn, B. Santos Burgos, T. O. Menteş, A.

Locatelli, F. Montaigne, and N. Rougemaille, *Kinetic Pathways to the Magnetic Charge Crystal in Artificial Dipolar Spin Ice*, Phys. Rev. B **90**, 220407 (2014).

[24] J. Drisko, S. Daunheimer, and J. Cumings, *FePd3 as a Material for Studying Thermally Active Artificial Spin Ice Systems*, Phys. Rev. B **91**, 224406 (2015).

[25] T. Dion, D. M. Arroo, K. Yamanoi, T. Kimura, J. C. Gartside, L. F. Cohen, H. Kurebayashi, and W. R. Branford, *Tunable Magnetization Dynamics in Artificial Spin Ice via Shape Anisotropy Modification*, Phys. Rev. B **100**, 054433 (2019).

[26] M. Tanaka, E. Saitoh, H. Miyajima, T. Yamaoka, and Y. Iye, *Magnetic Interactions in a Ferromagnetic Honeycomb Nanoscale Network*, Phys. Rev. B **73**, 052411 (2006).

[27] Y. Qi, T. Brintlinger, and J. Cumings, *Direct Observation of the Ice Rule in an Artificial Kagome Spin Ice,* Phys. Rev. B **77**, 094418 (2008).

[28] G. Möller and R. Moessner, *Magnetic Multipole Analysis of Kagome and Artificial Spin-Ice Dipolar Arrays*, Phys. Rev. B **80**, 140409 (2009).

[29] J. Li, X. Ke, S. Zhang, D. Garand, C. Nisoli, P. Lammert, V. H. Crespi, and P. Schiffer, *Comparing Artificial Frustrated Magnets by Tuning the Symmetry of Nanoscale Permalloy Arrays*, Phys. Rev. B **81**, 092406 (2010).

[30] W. R. Branford, S. Ladak, D. E. Read, K. Zeissler, and L. F. Cohen, *Emerging Chirality in Artificial Spin Ice*, Science. **335**, 1597 (2012).

[31] J. C. Gartside, D. M. Arroo, D. M. Burn, V. L. Bemmer, A. Moskalenko, L. F. Cohen, and W. R. Branford, *Realization of Ground State in Artificial Kagome Spin Ice via Topological Defect-Driven Magnetic Writing*, Nat. Nanotechnol. **13**, 53 (2018).

[32] L. J. Heyderman and R. L. Stamps, *Artificial Ferroic Systems: Novel Functionality from Structure, Interactions and Dynamics*, J. Phys. Condens. Matter **25**, 363201 (2013).

[33] N. Rougemaille and B. Canals, *Cooperative Magnetic Phenomena in Artificial Spin Systems: Spin Liquids, Coulomb Phase and Fragmentation of Magnetism – a Colloquium*, Eur. Phys. J. B **92**, 62 (2019).

[34] C. Nisoli, R. Moessner, and P. Schiffer, *Colloquium: Artificial Spin Ice: Designing and Imaging Magnetic Frustration*, Rev. Mod. Phys. **85**, 1473 (2013).

[35] A. S. Wills, R. Ballou, and C. Lacroix, *Model of Localized Highly Frustrated Ferromagnetism: The Kagomé Spin Ice*, Phys. Rev. B **66**, 144407 (2002).

[36] V. Schánilec, B. Canals, V. Uhlíř, L. Flajšman, J. Sadílek, T. Šikola, and N. Rougemaille, *Bypassing Dynamical Freezing in Artificial Kagome Ice,* Phys. Rev. Lett. **125**, 057203 (2020).

[37] K. Hofhuis, S. Skjærvø, A. Kleibert, P. S. Institut, and L. Heyderman, *Real-Space Imaging of Phase Transitions in Bridged Artificial Kagome Spin Ice*, Nat. Phys. (2022). https://doi.org/10.1038/s41567-022-01564-5

[38] C. Nisoli, R. Wang, J. Li, W. F. McConville, P. E. Lammert, P. Schiffer, and V. H. Crespi, *Ground State Lost but Degeneracy Found: The Effective Thermodynamics of Artificial Spin Ice*, Phys. Rev. Lett. **98**, 217203 (2007).

[39] J. P. Morgan, A. Stein, S. Langridge, and C. H. Marrows, *Thermal Ground-State Ordering and Elementary Excitations in Artificial Magnetic Square Ice*, Nat. Phys. **7**, 75 (2011).

[40] A. Farhan, P. M. Derlet, A. Kleibert, A. Balan, R. V. Chopdekar, M. Wyss, J. Perron, A.

Scholl, F. Nolting, and L. J. Heyderman, *Direct Observation of Thermal Relaxation in Artificial Spin Ice*, Phys. Rev. Lett. **111**, 057204 (2013).

[41] V. Kapaklis, U. B. Arnalds, A. Farhan, R. V. Chopdekar, A. Balan, A. Scholl, L. J. Heyderman, and B. Hjörvarsson, *Thermal Fluctuations in Artificial Spin Ice*, Nat. Nanotechnol. **9**, 514 (2014).

[42] V. M. Parakkat, G. M. Macauley, R. L. Stamps, and K. M. Krishnan, *Configurable Artificial Spin Ice with Site-Specific Local Magnetic Fields*, Phys. Rev. Lett. **126**, 017203 (2021).

[43] J. C. Gartside, A. Vanstone, T. Dion, K. D. Stenning, D. M. Arroo, H. Kurebayashi, and W. R. Branford, *Reconfigurable Magnonic Mode-Hybridisation and Spectral Control in a Bicomponent Artificial Spin Ice*, Nat. Commun **12**, 2488 (2021).

[44] S. Lendinez, M. T. Kaffash, and M. B. Jungfleisch, *Emergent Spin Dynamics Enabled by Lattice Interactions in a Bicomponent Artificial Spin Ice*, Nano Lett. **21**, 1921 (2021).

[45] See Supplemental Material at XXX for additional information and figures.

[46] A. Vansteenkiste, J. Leliaert, M. Dvornik, M. Helsen, F. Garcia-Sanchez, and B. Van Waeyenberge, *The Design and Verification of MuMax3*, AIP Adv. **4**, 107133 (2014).

[47] E. Östman, H. Stopfel, I. A. Chioar, U. B. Arnalds, A. Stein, V. Kapaklis, and B. Hjörvarsson, *Interaction Modifiers in Artificial Spin Ices*, Nat. Phys. **14**, 375 (2018).

[48] A. J. MacDonald, P. C. W. Holdsworth, and R. G. Melko, *Classical Topological Order in Kagome Ice*, J. Phys. Condens. Matter **23**, 164208 (2011).

[49] F. S. Nascimento, L. A. S. Mól, W. A. Moura-Melo, and A. R. Pereira, *From Confinement*

to Deconfinement of Magnetic Monopoles in Artificial Rectangular Spin Ices, New J. Phys. **14**, 115019 (2012).

[50] I. R. B. Ribeiro, F. S. Nascimento, S. O. Ferreira, W. A. Moura-Melo, C. A. R. Costa, J. Borme, P. P. Freitas, G. M. Wysin, C. I. L. De Araujo, and A. R. Pereira, *Realization of Rectangular Artificial Spin Ice and Direct Observation of High Energy Topology*, Sci. Rep. **7**, 13982 (2017).

[51] S. Lendinez and M. B. Jungfleisch, *Magnetization Dynamics in Artificial Spin Ice*, J. Phys. Condens. Matter **32**, 013001 (2020).

[52] S. Gliga, E. Iacocca, and O. G. Heinonen, *Dynamics of Reconfigurable Artificial Spin Ice: Toward Magnonic Functional Materials*, APL Mater. **8**, 040911 (2020).

[53] M. Fuchs, P. Liu, T. Schwemmer, G. Sangiovanni, R. Thomale, C. Franchini, and D. D. Sante, *Kagome metal-organic frameworks as a platform for strongly correlated electrons*, J. Phys. Mater. 3 025001 (2020).

[54] D. Z. Rocklin, S. Zhou, K. Sun, and X. Mao, *Transformable topological mechanical metamaterials*, Nat. Commun. 8, 14201 (2017)

[55] C. Coulais, E. Teomy, K. de Reus, Y. Shokef and M. van Hecke, *Combinatorial design of textured mechnical metamaterials*, Nature 535, 529 (2016)

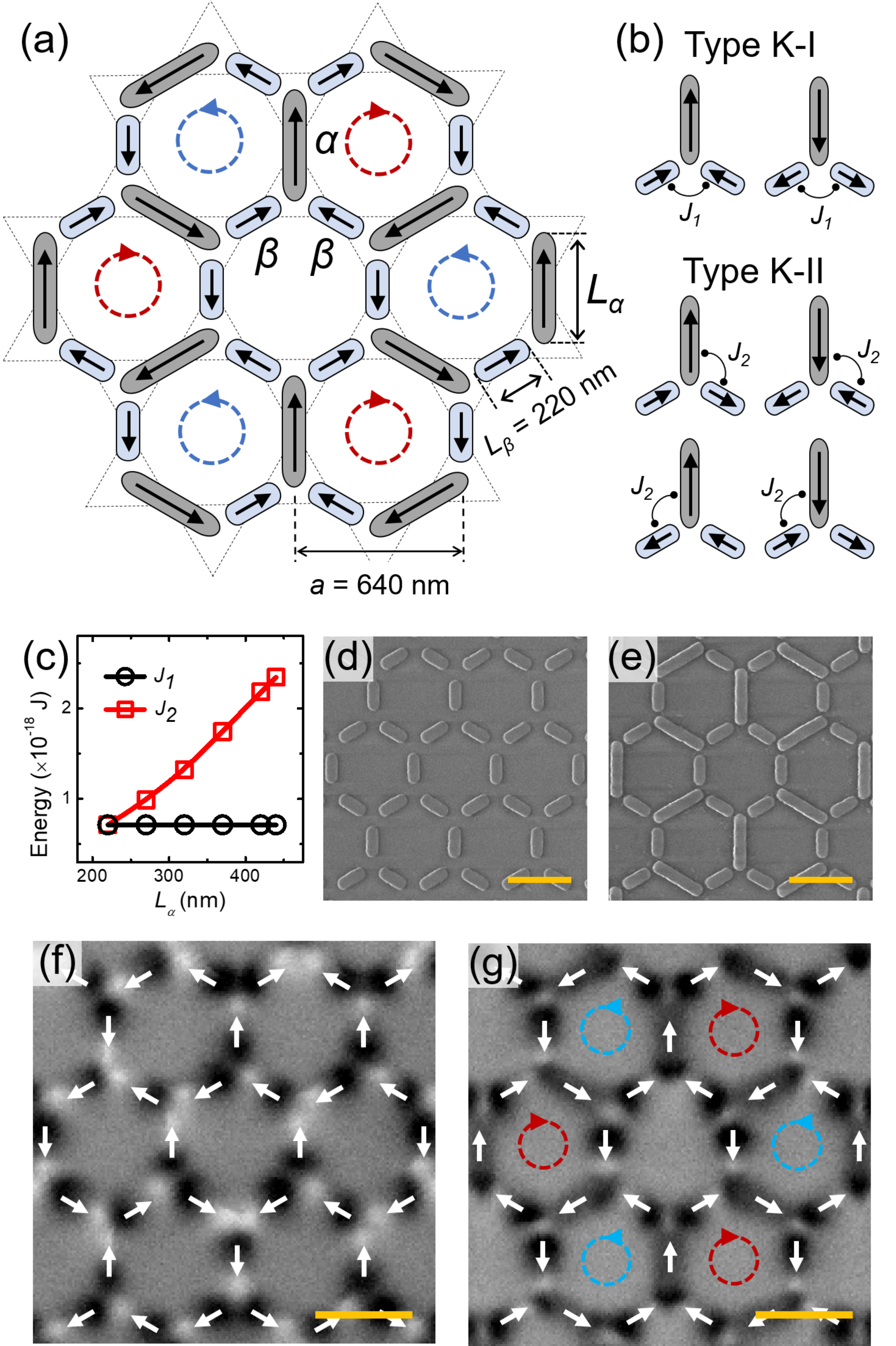

(a)
α
β
β
L_α
L_β = 220 nm
a = 640 nm
(b)
Type K-I
J_1
J_1
Type K-II
J_2
J_2
J_2
J_2
(c)
J_1
J_2
Energy (×10^{-18} J)
2
1
200
300
400
L_α (nm)
(d)
(e)
(f)
(g)

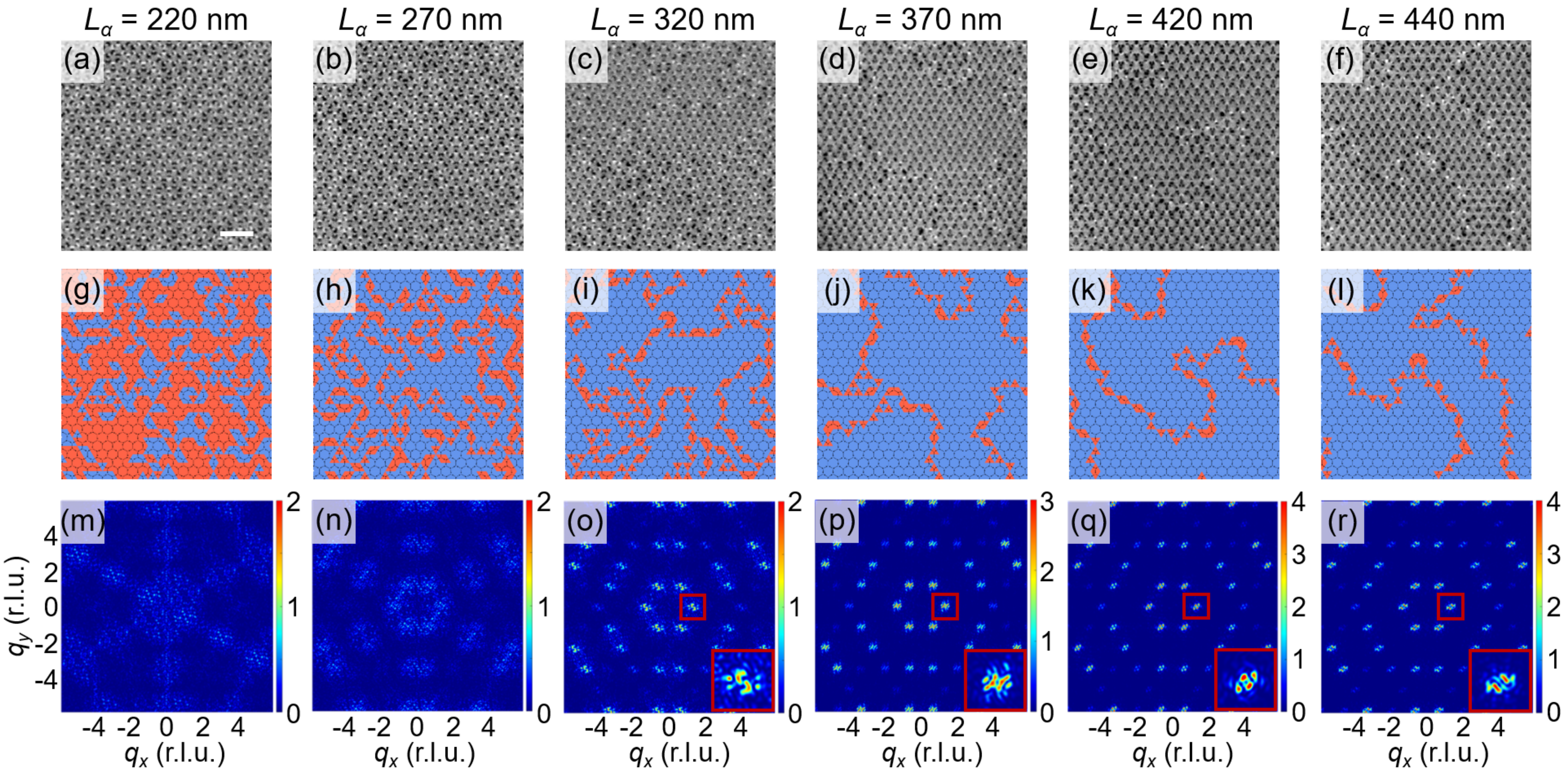

L_α = 220 nm
L_α = 270 nm
L_α = 320 nm
L_α = 370 nm
L_α = 420 nm
L_α = 440 nm
(a)
(b)
(c)
(d)
(e)
(f)
(g)
(h)
(i)
(j)
(k)
(l)
(m)
(n)
(o)
(p)
(q)
(r)
q_y (r.l.u.)
q_x (r.l.u.)

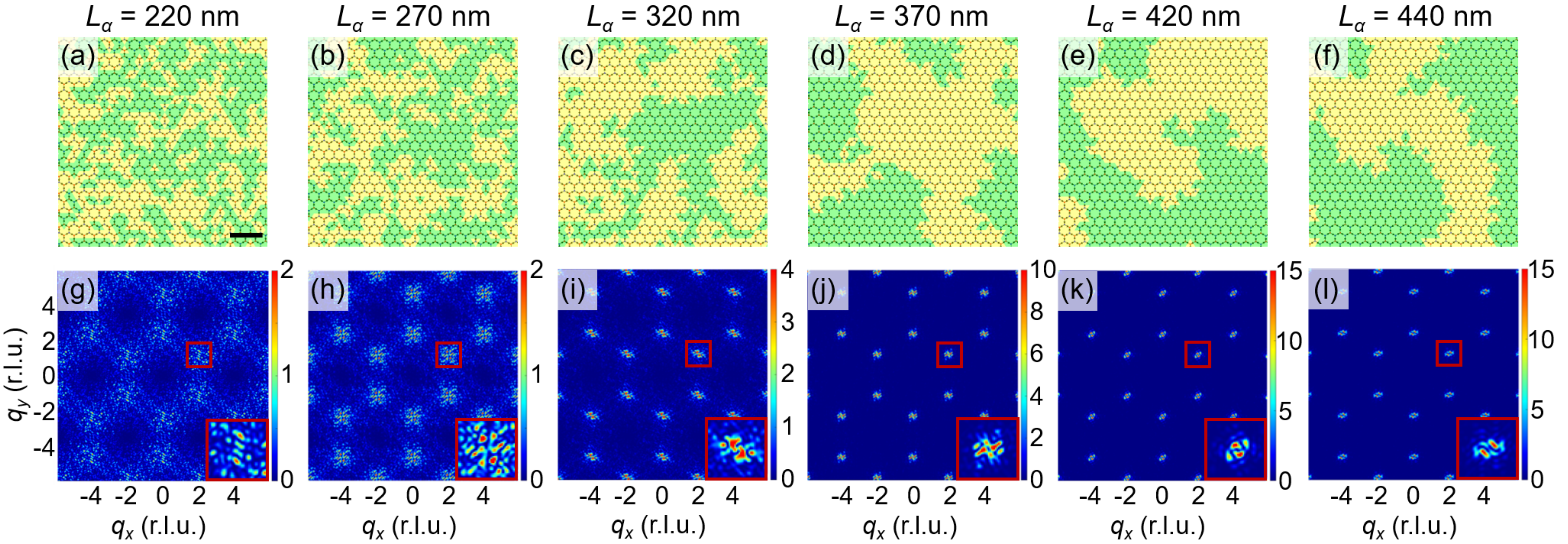

L_α = 220 nm
L_α = 270 nm
L_α = 320 nm
L_α = 370 nm
L_α = 420 nm
L_α = 440 nm
(a)
(b)
(c)
(d)
(e)
(f)
(g)
(h)
(i)
(j)
(k)
(l)
q_y (r.l.u.)
q_x (r.l.u.)
-4 -2 0 2 4